PCCP

PAPER

View Article Online
View Journal | View Issue

Cite this: *Phys. Chem. Chem. Phys.*, 2025, **27**, 3873

Two-photon absorption of BODIPY, BIDIPY, GADIPY, and SBDIPY†

Ismael A. Elayan, * Mingmin Zhou and Alex Brown *

Substituted boron-dipyrromethene compounds (BODIPYs) have gained significant attention due to their tunable photophysical properties, including two-photon absorption (2PA), a nonlinear optical process where two photons are absorbed simultaneously. The tuning of BODIPY's photophysical properties has recently led to the synthesis of pnictogen-containing derivatives, such as SBDIPY and BIDIPY, where boron is replaced by antimony (Sb) or bismuth (Bi), respectively, as well as other analogues like GADIPY, which contain gallium (Ga). This study presents a computational investigation into their 2PA properties, exploring the impact of various substitutions across these systems. The 2PA cross-sections (σ^{2PA}), electronic excitation energies (ΔE), and dipole moments (μ_{00}, μ_{11}, μ_{01}, $\Delta\mu$) were computed for 18 DIPY chromophores in the gas-phase with time-dependent density-functional theory (TD-DFT) using several functionals (CAM-B3LYP, ωB97X, M06-2X, M11, and MN15), and then compared to second-order approximate coupled-cluster with the resolution-of-identity approximation (RI-CC2) results. The computed mean absolute errors were small, with the MN15, CAM-B3LYP, and M06-2X functionals being among the best-performing for the properties analyzed. In general, for the parent (unsubstituted) compounds, replacing the core atom in DIPY chromophores results in negligible changes to their σ^{2PA}. However, extending the conjugation through the addition of phenyl substituents significantly increases σ^{2PA} values, and the nature of the core atom impacts the magnitude of this enhancement.

Received 11th October 2024,
Accepted 27th January 2025

DOI: 10.1039/d4cp03915g

rsc.li/pccp

Introduction

The class of boron–dipyrromethene (BODIPY) derivatives has attracted broad interest as a key group of stable organic fluorophores.[1,2] The simplicity of BODIPYs' chemical composition, consisting of boron difluoride linked to conjugated dipyrromethene,[3–5] allows for their tunability through the availability of a number of different sites accessible to a wide variety of substituents. These substitutions can lead to desirable photophysical attributes including photochemical stability, large extinction coefficients, and large quantum yields.[2,6,7] Since their initial discovery in 1968,[3] BODIPYs have evolved significantly,[6,7] with an expansion of derivatives emerging from their tunable photophysical characteristics through chemical structure alterations. These modifications include changes to the system's size by varying the number of adjacent rings and introducing different functional group substituents, thereby resulting in altered chemical and physical characteristics.[8–12] This chemical diversity has led to their widespread application in various fields,[1,2,6,7] including photodynamic therapy,[13] biomolecular labeling,[14] chemiluminescence,[15] as laser dyes,[16] fluorescent dyes and probes,[17,18] biological imaging,[19,20] and two-photon absorption.[21–24]

Earlier alterations of BODIPYs included the introduction of various functional groups at the *meso*-, α-, and β-positions, including alkyl, aryl, alkyne, and alkoxide;[2,25–27] see Fig. 1 for illustration of these positions. Such adjustments have been shown to influence the fluorescence and absorption properties of the dyes, which also result in changes to their solubility, stability, and effectiveness for use in bio-imaging.[2,6] Furthermore, a promising strategy involves integrating heavy atoms into the core of BODIPY chromophores, significantly impacting their luminescence and optoelectronic features by affecting emission and absorption spectra as well as quantum yields.[28,29] This approach has recently been demonstrated by substituting boron atoms with heavier elements such as gallium, phosphenium, antimony, bismuth, germanium, tin, and arsenic, leading to the development of GADIPY, PHODIPY, SBDIPY, BIDIPY, GEDIPY, SNDIPY, and ASDIPY chromophores, respectively.[30–34] In general, these conjugated DIPY frameworks, which have different substituents at *meso*-, α-, and β-positions, are linked either to dichloride, dibromide, or difluoride, see Fig. 1.

In 2019, the synthesis and optical characterization of BODIPY analogues were first reported, specifically GADIPY

Department of Chemistry, University of Alberta, Edmonton, Alberta, Canada T6G 2G2. E-mail: elayan@ualberta.ca, alex.brown@ualberta.ca

† Electronic supplementary information (ESI) available: Cartesian coordinates of the optimized geometries, excitation energies, dipole moments, 2PA cross-sections, 2PA transition strengths, mean absolute errors, and mean signed errors. See DOI: https://doi.org/10.1039/d4cp03915g

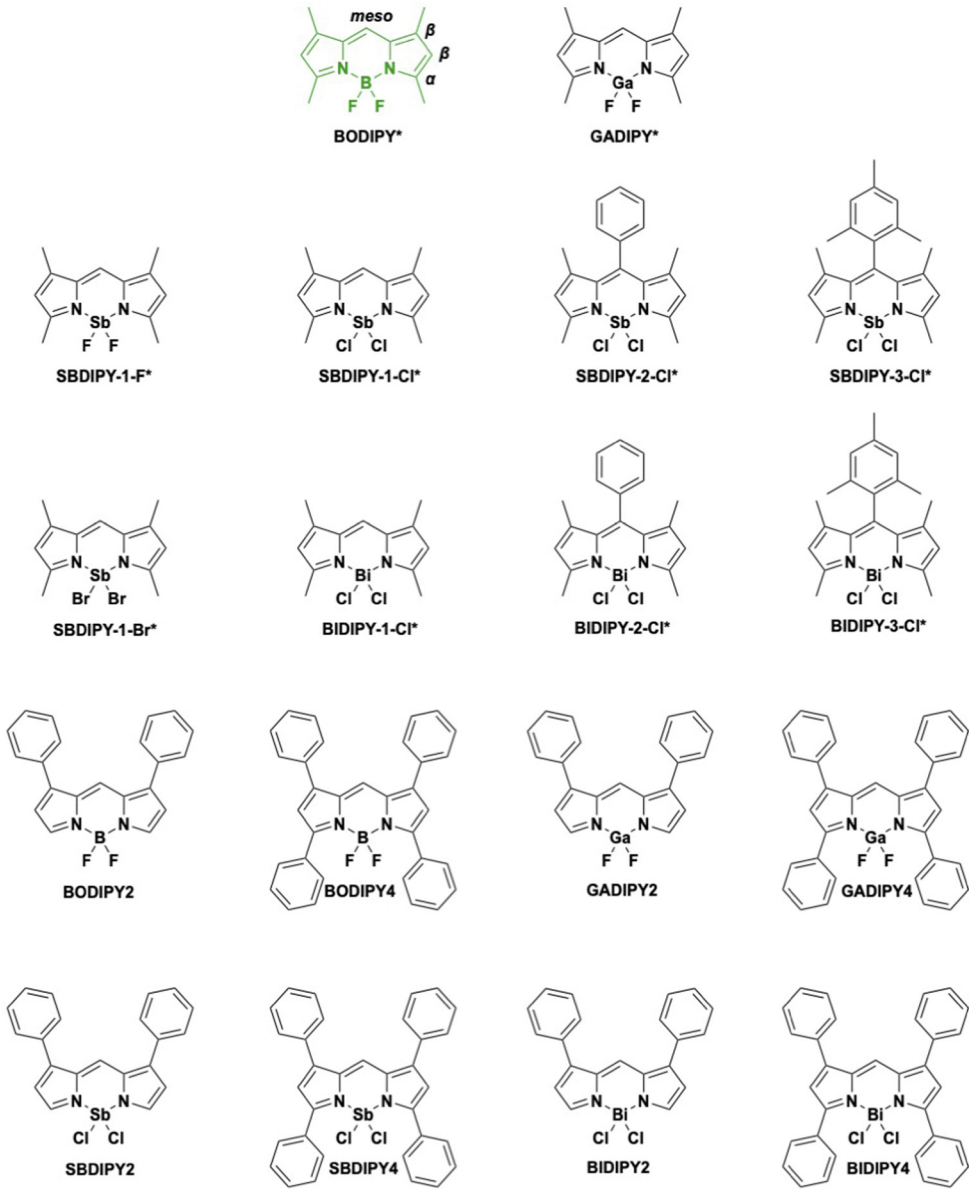

Fig. 1 BODIPY analogues investigated in this study, with the core structure highlighted in green. The first ten analogues, as indicated with an asterisk, have been experimentally reported.[30–32,34]

and PHODIPY, where the former is linked to dichloride and the latter to phenyl.[30] In particular, GADIPY exhibited photostability coupled with an intense green fluorescence and quantum yield (Φ) of 0.91. On the other hand, while PHODIPY demonstrates a high $\Phi = 0.80$ in dichloromethane, it was found to be cationic due to the phenylphosphenium ion fragment used in its synthesis, making it inherently unstable and leading to its decomposition into phosphine. Subsequent to these initial discoveries,[30] the GEDIPY radical, substituted at the *meso*- and α-positions and characterized by electron delocalization across the DIPY backbone and germanium center, was reported to exhibit chemical stability due to this delocalization.[34] Furthermore, Liu *et al.*[32] expanded the scope of pnictogen-DIPYs by introducing SBDIPY and BIDIPY, the heavier counterparts in the DIPY series, linked to dichloride, see Fig. 1. The chromophore cores of SBDIPY and BIDIPY have been further modified with the introduction of difluoride and dibromide substitutions in dichloromethane,[31] extending the versatility of these compounds. Furthermore, the structures diverge from those identified by Liu *et al.*,[32] attributed to variations in alkylation or arylation at the *meso*-, α-, or β-positions,[31] resulting in different DIPY variants. A detailed discussion and comparison of the determined photophysical properties of the reported DIPY analogues can be found in the ESI.†

In recent developments, analogues of SNDIPY and ASDIPY, substituted at the *meso*- and α-positions, have also been successfully isolated in toluene,[33] expanding the family of these distinctive compounds. Similar to earlier findings for the heavier

pnictogen-DIPYs, the newly isolated analogues also exhibit low quantum yields with values of Φ = 0.033 for SNDIPY and Φ = 0.056 for ASDIPY. Therefore, this indicates that while these pnictogen-DIPYs are interesting due to their unique structures and the incorporation of different halogens, they are not as efficient in terms of photoluminescence when compared to some of the best-performing known analogues.[1,2] However, their photophysical properties can be tuned *via* substitution, or they may be useful for other purposes, *e.g.*, photodynamic therapy. The high Φ reported for GADIPY indicates its potential as a candidate for nonlinear optical applications, such as in two-photon absorption processes.

Two-photon absorption (2PA), a nonlinear optical process, enables the simultaneous absorption of two photons, which can be either of degenerate energy or non-degenerate energies.[35–37] Characterized by its quadratic dependence on light intensity and its ability to access longer wavelengths,[36,38] 2PA enhances spatial resolution and reduces photo-damage in biological contexts.[21] Therefore, it finds extensive application in bio-imaging and photodynamic therapy.[39–41] However, exploring 2PA probes presents the challenge of their inherently lower sensitivity as measured *via* 2PA probabilities compared to one-photon absorption. These 2PA probabilities are quantitatively expressed in terms of cross-sections (σ^{2PA}), measured in Göppert–Mayer (GM) units, where 1 GM corresponds to 10^{-50} cm^4 s molecule^{-1} photon^{-1}.[36,42] Furthermore, accurately determining absolute σ^{2PA} values presents experimental challenges,[41] primarily due to the need to assess various parameters involved in the experimental measurements.[38,43] Therefore, computational chemistry emerges as a pivotal tool for understanding and quantifying σ^{2PA} values, facilitating the exploration of 2PA probes and their corresponding photophysical properties.[37,44–49]

Over recent years, computational tools have improved our understanding of the photophysical characteristics associated with 2PA processes in BODIPY chromophores.[22,50–52] These studies include detailed examination of the relationship between the molecular design, particularly the modifications at the *meso*-, α-, and β-positions, and their impact on 2PA efficiency.[22,52,53] By tailoring these chromophores, the objective has been to comprehensively understand and improve their σ^{2PA},[54–57] thereby achieving higher values conducive to enhanced functionality. In particular, computational investigations of BODIPYs have revealed the influence of extended π-conjugation induced by various substituents on 2PA efficiencies, as well as the vital roles that molecular symmetry and planarity play in determining these efficiencies.[50,52,54–56] On the other hand, distortions from planarity, triggered by bulky substituents, can lead to a decrease in 2PA efficiency due to the disruption of π-electron delocalization.[52,54]

The above-mentioned novel DIPY chromophores (Fig. 1), characterized by the integration of heavier elements within their framework, remain unexplored in the context of their 2PA properties, both computationally and experimentally. The goal of this work is to provide a detailed analysis of the calculated σ^{2PA} values and to establish a qualitative framework for understanding how these values might be improved. Through the use of second-order approximate coupled-cluster with the resolution-of-identity approximation (RI-CC2)[58,59] and time-dependent density functional theory (TD-DFT) with CAM-B3LYP,[60–62] ωB97X,[63] M06-2X,[64] M11,[65] and MN15[66] functionals, we present a detailed examination of σ^{2PA}, excitation energies (ΔE), and key dipole moments (μ_{00}, μ_{11}, μ_{01}, and $\Delta\mu$) for the photoexcitation from the ground state, S_0, to the first electronic singlet excited state, S_1, across 18 DIPY chromophores (see Fig. 1).

Computational methods

The Cartesian coordinates for the chromophores GADIPY, SBDIPY-1-F, SBDIPY-1-Cl, SBDIPY-2-Cl, SBDIPY-3-Cl, SBDIPY-1-Br, BIDIPY-1-Cl, BIDIPY-2-Cl, and BIDIPY-3-Cl were obtained from Korzun *et al.*,[31] who employed the r^2 SCAN-3c method for geometry optimization.[67] Their computed geometries agree with the experimentally determined structures,[31] which can be seen from both the bond lengths and angles (Table S1, ESI†), particularly within the core structure, the core atom, and its linkage to the surrounding atoms. Across the DIPY derivatives, deviations between theoretical and experimental values for key bond lengths, such as C–N, C–C, Bi–Cl, Sb–Cl, and Sb–Br, remain minimal, typically within 0.01–0.03 Å. Similarly, bond angles, such as those involving the dipyrrin core and halogen substitutions, show a general agreement, with most deviations remaining below 2.0°. However, when considering the core atom bonding with the halogens, it is worth noting that the computed geometries assume a symmetrical arrangement of equivalent bond lengths, which sometimes leads to discrepancies when compared to experimental measurements. For example, in the BIDIPY derivatives, the computations predict similar bond lengths for Bi–Cl, while experimentally, these bonds differ by 0.47 Å in BIDIPY-1-Cl and 0.27 Å in BIDIPY-2-Cl, most likely, due to packing effects in the solid state. A similar observation is made for SBDIPY derivatives, where the computed values are identical but experimental results show differences; however, they do not exceed 0.06 Å. Overall, the computed trends in bond lengths and angles are reliable compared to the experimental ones.

In the experimental study,[31] BIDIPY-1-Cl, BIDIPY-2-Cl, and BIDIPY-3-Cl were obtained as dimers due to the presence of two bridging chlorides connecting two bismuth centers. In this work, we focused on the monomeric units, utilizing the Cartesian coordinates optimized for these species as previously provided.[31] The above-mentioned comparison of the optimized geometries with the experimentally determined structures generally demonstrates a reliable agreement. While intermolecular interactions, such as those forming dimers or aggregates, are crucial to solid-state behavior, they fall outside the scope of this study.

The rest of the geometries, where the substituted ones were based on previously commonly investigated derivatives,[50,52,54–57] were optimized using the PBE0/def2-SVP level of theory[68] utilizing Gaussian16.[69] This level of theory was selected in accordance with

the benchmark established by Momeni and Brown for BODIPYs.[70] The optimized geometries were confirmed to represent minima by the absence of imaginary frequencies in their vibrational frequency analysis. Differences in the selected optimization methods within the approach considered should not significantly influence the obtained findings. For example, our recent work[45] demonstrates that geometries optimized at one level of theory, coupled with excited-state calculations performed at another, result in minimal changes to absolute values while preserving qualitative trends. Similarly, another study of ours[46] showed that σ^{2PA} and ΔE values remain qualitatively consistent when comparing geometries optimized using different conditions, such as solvent-phase[37] *versus* gas-phase optimizations.[46] These observations confirm that minor variations in optimization protocols do not affect the trends or conclusions of such studies.

The electronic excitations, which involved transitions from S_0 to S_1, were computed using both TD-DFT[71,72] and wavefunction theory (WFT) (RI-CC2),[59] using TURBOMOLE 7.7.1.[73–75] The excited state calculations were performed in the gas phase employing the aug-cc-pVDZ basis set,[76,77] a choice validated by its adequacy for capturing 2PA intensity details efficiently.[47,78] Furthermore, the ΔE values for the experimentally available systems were computed using TD-DFT in dichloromethane with the conductor-like screening model (COSMO) for continuum solvation.[79] The solvent parameters applied in these calculations included a radius of 1.3 (default), a dielectric constant of 8.93, and a refractive index of 1.4244. These calculations presumed linearly polarized light, with photophysical properties obtained using the length gauge. However, it is crucial to acknowledge that for BODIPY compounds, discrepancies have been observed between TD-DFT-based predictions of excited state properties, such as ΔE, and those derived from experimental data or WFT.[70,80–85] Such deviations are due to the multi-reference character of the BODIPYs, role of double excitations, and the challenge of accurately addressing electron correlation in TD-DFT.[70,85]

The computations of 2PA cross-sections in macroscopic units (GM), involve the transformation of the transition strength term, δ^{2PA}, into σ^{2PA} where the following formula is used,[86]

$$\sigma^{2PA} = \frac{N\pi^2 a_0^2 \alpha (2\omega)^2}{c\Gamma}\delta^{2PA}. \quad (1)$$

In eqn (1), $N = 1$ (for a single beam experiment), a_0 denotes the Bohr radius, α is the fine-structure constant, ω represents the photon energy, which is obtained from $\frac{\Delta E}{2}$, c is the speed of light, and Γ indicates the lifetime broadening, set at 0.1 eV. However, the expression for δ^{2PA}, varies based on the computational method, TD-DFT or RI-CC2. When employing TD-DFT, the formula for δ^{2PA} is defined as,[86]

$$\delta^{2PA} = \frac{1}{15}\sum_{\alpha\beta}\left[S_{\alpha\alpha}S^*_{\beta\beta} + 2S_{\alpha\beta}S^*_{\alpha\beta}\right] \quad (2)$$

where the two-photon transition matrix element, $S_{\alpha\beta}$ ($\alpha, \beta = x, y, z$), is expressed as,

$$S_{\alpha\beta} = \sum_n \left[\frac{\langle 0|\mu_\alpha|n\rangle\langle n|\mu_\beta|f\rangle}{\omega_n - \omega_1} + \frac{\langle 0|\mu_\beta|n\rangle\langle n|\mu_\alpha|f\rangle}{\omega_n - \omega_2}\right]. \quad (3)$$

In this expression, the Cartesian dipole moment components, $\mu_{\alpha,\beta}$, along with the energy of the excited state, ω_n, are described in terms of the excitation process from the ground state $|0\rangle$ to an intermediate state $|n\rangle$. However, in the RI-CC2 approach, the use of a Jacobian non-symmetric matrix differentiates the left ($\mathscr{L}$) and right ($\mathscr{R}$) components of the tensor $S_{\alpha\beta}$,[47,59] where both, in terms of Cartesian coordinates where μ are provided as relaxed properties, are expressed as,

$$S^{\mathscr{L}}_{xy} = S^{xy}_{0\leftarrow f} = \sum_n \left[\frac{\langle 0|\mu_x|n\rangle\langle n|\mu_y|f\rangle}{\omega_n - \omega_1} + \frac{\langle 0|\mu_y|n\rangle\langle n|\mu_x|f\rangle}{\omega_n - \omega_2}\right] \quad (4)$$

$$S^{\mathscr{R}}_{xy} = S^{xy}_{f\leftarrow 0} = \sum_n \left[\frac{\langle f|\mu_x|n\rangle\langle n|\mu_y|0\rangle}{\omega_n - \omega_1} + \frac{\langle f|\mu_y|n\rangle\langle n|\mu_x|0\rangle}{\omega_n - \omega_2}\right]. \quad (5)$$

Thus, the calculation of $S_{\alpha\beta}$ necessitates incorporating both the left and right eigenvectors. This integration results in a different expression, compared to TD-DFT (eqn (2)), for δ^{2PA}, where,[59,87]

$$\delta^{2PA}_{0f} = \frac{1}{15}\sum_\alpha\sum_\beta\left[S^{\alpha\alpha}_{f\leftarrow 0}S^{\beta\beta}_{0\leftarrow f} + S^{\alpha\beta}_{f\leftarrow 0}S^{\alpha\beta}_{0\leftarrow f} + S^{\alpha\beta}_{f\leftarrow 0}S^{\beta\alpha}_{0\leftarrow f}\right] \quad (6)$$
$$\alpha, \beta \in x, y, z.$$

This study focuses on calculating ΔE, σ^{2PA}, and μ values for recently synthesized DIPY chromophores (Fig. 1), while also investigating substituent effects on these properties. The study employs both quantitative and qualitative analyses, with an emphasis on qualitative investigation using response theory. The RI-CC2 method[59] serves as a reference point to TD-DFT results, including the functionals CAM-B3LYP,[62] ωB97X,[63] M06-2X,[64] M11,[65] and MN15.[66] The effectiveness of RI-CC2 has been previously confirmed,[48,88,89] demonstrating that the computed 2PA results from RI-CC2 closely align with those obtained from other wavefunction-based methods such as CCSD, EOM-CCSD, and CC3.

Until early 2024, CAM-B3LYP had predominantly been the preferred functional for studying the 2PA photophysical properties of various chromophores, supported by benchmarks across different functionals, involving the generalized gradient approximation (GGA), including the PBE and BLYP functionals; hybrid-GGA (H-GGA) functionals, such as PBE0, B1LYP, B3LYP, and BHandHLYP; and range-separated hybrid-GGA (RSH-GGA) functionals like LC-BLYP and CAM-B3LYP, with a general recommendation for RSH-GGA functionals.[47,48,78,90,91] Recently, an extensive evaluation of 40 functionals, including a broad range of *meta*-GGA (M-GGA) and hybrid M-GGA (HM-GGA) functionals,[92] showed that functionals like M06-2X and MN15 closely correlate with RI-CC2, featuring low mean relative errors. Furthermore, in a more recent work of ours,[46] we analyzed 19 DFT functionals and found that M11, M06-2X, and ωB97X, among

others, exhibit the best correlations and the lowest mean absolute errors, relative to RI-CC2. In line with recent recommendations,[46,92] the functionals CAM-B3LYP, ωB97X, M06-2X, M11, and MN15 have been chosen for our computational analysis. Furthermore, to focus the discussion primarily on the selected dyes rather than on the computational methods themselves, we have opted to use MN15 as the primary functional for the detailed analysis and discussions, which will be compared to RI-CC2. However, the performance of other functionals will be briefly reviewed in the context of their efficacy in predicting the photophysical properties of the investigated DIPYs.

Results and discussion

This study primarily addresses qualitative trends in response to challenges previously noted in quantifying σ^{2PA} and accurately calculating dipole moment properties.[48,90,91] A recurring challenge is the underestimation of σ^{2PA} values by TD-DFT compared to those obtained through experimental measurements and wavefunction methods, RI-CC2 and EOM-CCSD.[46,93,94] Furthermore, the computation of 2PA properties depends on the specific functionals used, whether for σ^{2PA} (eqn (1)) or δ^{2PA} (eqn (2)), and our recent findings show how the conclusions drawn can vary,[46] affecting both quantitative assessments and qualitative interpretations. However, given that σ^{2PA} is the parameter typically measured in experiments,[38] the discussion in the present work primarily focuses on its calculated values. Moreover, the relative performance of functionals in predicting δ^{2PA} is briefly addressed in the computed values of σ^{2PA} section. It is essential to note that σ^{2PA} results from the product of δ^{2PA} and ω (eqn (1)). This dependency can introduce errors from each contributing parameter, possibly resulting in error cancellation for the reported values of σ^{2PA}.

In the investigation of BODIPY analogues and their ΔE values, various functionals have been explored, including double-hybrid functionals.[70,85,95,96] In general, it was observed that chemical modifications, such as substituting methyl groups with hydrogens,[97] impact the electronic properties, leading to changes in the charge transfer characteristics, ultimately resulting in red-shifted dyes. Since several studies have examined the computed values of ΔE for different BODIPYs, as well as some of the studied DIPYs herein (Fig. 1),[31] the computed values of ΔE presented here will be briefly discussed and compared to previously reported values, particularly experimental ones.[30–32,34]

The analysis of the experimental ΔE values (as approximated from measured λ_{max}) for the synthesized DIPYs and their comparison to the computed values (see Table 1 and Fig. S1, ESI†), demonstrates that the RI-CC2 values exhibit the lowest mean absolute error (MAE) of 0.36 eV. Thus, while RI-CC2 systematically overestimates the values of ΔE, the average magnitude of these errors is relatively low compared to TD-DFT results. For the TD-DFT (CAM-B3LYP, ωB97X, M06-2X, M11, and MN15) results, the MAEs range from 0.43 to 0.47 eV, which are slightly higher compared to RI-CC2. As expected, the overestimation of ΔE is consistent with earlier findings for BODIPY systems.[70,85] Given that RI-CC2 has been identified as having the lowest MAE relative to experimental findings (Table 1), it serves as a benchmark to assess the MAEs of the TD-DFT results. The discrepancies observed between RI-CC2 and experimental findings can be (partially) attributed to vibronic effects and the environmental conditions (solvent); these effects are in addition to the known challenges of capturing the electronic structure of BODIPYs correctly.[70,82,85] Since the simulations only consider vertical excitations and neglect vibronic effects, and are conducted in the gas phase, they are inherently limited in achieving quantitative agreement with experimental results.[70,80,82,98] On the other hand, it is clear that the RI-CC2 method qualitatively aligns with the experimental results, in contrast to the examined TD-DFT functionals. For example, the experimental data show a slight decrease in ΔE from 2.46 eV for BIDIPY-1-Cl to 2.45 eV for both BIDIPY-2-Cl and BIDIPY-3-Cl, and RI-CC2 results accurately reproduce this trend. This qualitative agreement is also observed for other chromophores, such as the increase in ΔE when transitioning from BODIPY to GADIPY. Therefore, RI-CC2 can be regarded as a benchmark for the TD-DFT methods.

In the analysis of the experimental ΔE values measured in dichloromethane and their comparison to the computed values using the COSMO solvation model (Table S2 and Fig. S2) in the ESI,† it is clear that the inclusion of solvent effects slightly improves the agreement with experimental data compared to gas-phase simulations. This improved agreement is due to the lower computed ΔE values in solvent relative to gas-phase, where there is a general decrease in the obtained values within 0.12 eV. Among the investigated functionals, the MAEs range from 0.33 to 0.37 eV, with M11 showing the lowest MAE of 0.33 eV, closely followed by MN15 and ωB97X (both at 0.34 eV). These values indicate that solvent effects mitigate some discrepancies previously observed in the gas-phase calculations. However, our earlier study suggests that variations in the surrounding solvent environment exert only a minimal influence on the resulting values of ΔE.[70] While the experimentally observed trends are reproduced by RI-CC2 in gas-phase calculations, they remain inadequately captured by the other functionals.

Table 1 Values of ΔE (eV) and mean absolute errors (MAE) of the experimentally available (measured in dichloromethane) DIPY chromophores of interest. Computational results use aug-cc-pVDZ basis set and are in the gas-phase

Dyes	Expt.[ab]	RICC2	CAM-B3LYP	ωB97X	M06-2X	M11	MN15
BODIPY[a]	2.46	2.80	2.91	2.88	2.90	2.87	2.89
GADIPY[a]	2.51	2.91	2.99	2.97	2.99	2.95	2.97
SBDIPY-1-F[b]	2.50	2.85	2.95	2.92	2.94	2.91	2.92
SBDIPY-1-Cl[b]	2.47	2.83	2.92	2.89	2.91	2.88	2.89
SBDIPY-3-Cl[b]	2.47	2.82	2.94	2.92	2.92	2.91	2.89
SBDIPY-1-Br[b]	2.46	2.81	2.90	2.88	2.89	2.87	2.87
BIDIPY-1-Cl[b]	2.46	2.83	2.93	2.90	2.92	2.89	2.89
BIDIPY-2-Cl[b]	2.45	2.82	2.96	2.95	2.95	2.93	2.92
BIDIPY-3-Cl[b]	2.45	2.80	2.94	2.93	2.93	2.91	2.89
MAE	**0.00**	**0.36**	**0.47**	**0.45**	**0.46**	**0.43**	**0.43**

[a] Wan *et al.*[30] [b] Korzun *et al.*[31]

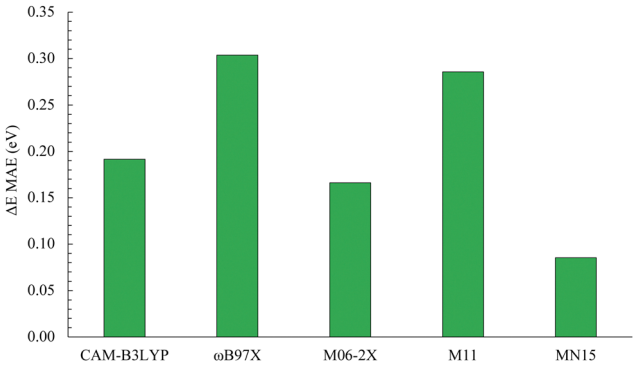

Fig. 2 The computed MAEs of ΔE (eV) for the 18 DIPY chromophores, relative to RI-CC2. The computed absolute values are given in Table S3 (ESI†).

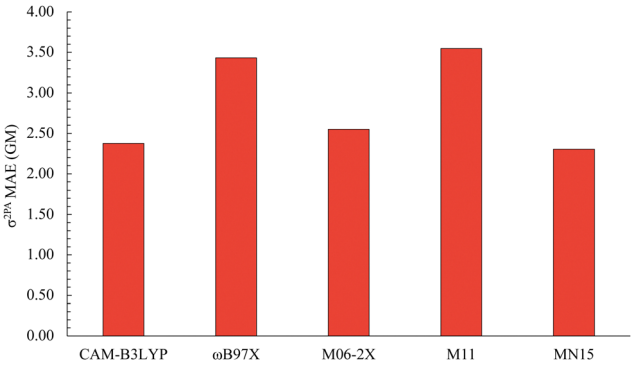

Fig. 3 The computed MAEs of σ^{2PA} (GM) for the DIPY chromophores, relative to RI-CC2. The computed absolute values are given in Table S3 (ESI†).

It is worth noting that the RI-CC2 calculations, despite being performed in the gas phase (MAE = 0.36 eV), remain comparable to the TD-DFT functionals when solvent effects are included (MAEs range from 0.34 to 0.37 eV). Moreover, RI-CC2 reliably reproduces the experimentally observed qualitative trends, such as variations in ΔE across different DIPY chromophores.

The quantitative MAEs are derived from the analysis of 9 out of the 18 investigated DIPYs, *i.e.*, those that have been synthesized and experimentally characterized. Further examination, detailed in Table S3 (ESI†), incorporating the additional dyes and (now) comparing the computed results relative to RI-CC2, rather than experiment, also reveals MN15 as the method with the lowest MAE of 0.09 eV. The comprehensive analysis, encompassing all investigated dyes and functionals, is depicted in Fig. 2, with the numerical values presented in Table S3 (ESI†). Thus, the discussion will primarily focus on the results obtained from RI-CC2 and MN15, given that the values of σ^{2PA} using MN15, relative to RI-CC2, also exhibit the lowest MSEs (Table S3, ESI†).

The computed values of σ^{2PA}

To date, there have been no experimental measurements of σ^{2PA} for the investigated systems, which shows the importance of using computational chemistry to study their 2PA properties. Drawing from recent studies,[46,92] the best-performing functionals, M06-2X, M11, MN15, ωB97X, and CAM-B3LYP, have been assessed for their efficacy in analyzing σ^{2PA} for the investigated chromophores by comparing their computed MAEs, when benchmarked relative to RI-CC2. The functional that shows the smallest MAE is then used for detailed quantitative and qualitative analysis, with a preference for qualitative exploration, *i.e.*, how is σ^{2PA} changed upon substituting boron and/or adding substituents.

In general, the values of σ^{2PA} calculated at different levels of theory are relatively low, with observed values between 0.30 and 44.00 GM, see Table S3 in the ESI.† The MAEs associated with these calculations range from 2.31 to 3.55 GM, suggesting that the functionals provide fairly consistent results with slight variations. However, the aim is to select a single functional for analysis to focus the discussion on the computed quantities rather than the explicit performance of functionals, which has been thoroughly discussed recently.[46,47,92] Fig. 3 presents the computed MAEs of σ^{2PA} relative to RI-CC2 for the functionals evaluated.

Regarding functional performance, MN15 achieves the best performance relative to RI-CC2, which is reflected through the lowest MAE of 2.31 GM. Similarly, both CAM-B3LYP and M06-2X perform well, with MAEs of 2.38 GM and 2.55 GM, respectively. In contrast, M11 and ωB97X exhibit higher deviations, with MAEs of 3.55 GM and 3.43 GM, respectively, displaying the largest inconsistencies with RI-CC2 among the investigated functionals. These findings are in agreement with the MAEs computed for ΔE, see Fig. 2. This comparative analysis of the MAEs for both ΔE and σ^{2PA} confirms that MN15 is the best-performing functional for these properties among the tested functionals. Furthermore, CAM-B3LYP remains a robust alternative with good performance, whereas M06-2X exhibits moderate accuracy. However, M11 and ωB97X are consistently identified as the least accurate functionals within this work. Therefore, based on this analysis, the discussion will focus on the numerical values of σ^{2PA} computed using RI-CC2 and MN15 for the studied DIPY chromophores.

The RI-CC2 calculations for σ^{2PA} across various DIPY chromophores reveal the significant effects of different substituents on these values. Starting with the base structure, BODIPY, the σ^{2PA} value is relatively low at 0.58 GM. Switching to GADIPY results in a slight increase to 0.60 GM, indicating that replacing boron with gallium has a minimal impact on the values of σ^{2PA}. On the other hand, substitutions involving antimony, particularly when paired with different halogens, show varied effects: SBDIPY-1-F, SBDIPY-1-Cl, SBDIPY-1-Br, which are unsubstituted DIPY molecules, show decreased σ^{2PA} values of 0.51, 0.46, 0.43 GM, respectively. Phenyl substitutions (at the *meso*-position), as observed in SBDIPY-2-Cl and SBDIPY-3-Cl, increase the values very modestly to 0.68 GM. Furthermore, similar trends are observed in BIDIPY derivatives: BIDIPY-1-Cl computed value σ^{2PA} = 0.45 GM is relatively low, while BIDIPY-2-Cl and BIDIPY-3-Cl exhibit (slightly) higher values of 0.68 GM and 0.64 GM, respectively. Although the values are low, the emphasis is on the changes in their magnitudes rather than the specific values themselves. Overall, and perhaps

unsurprisingly, the σ^{2PA} values of the parent DIPY compounds are small.

On the other hand, extending the conjugation of the chromophore core, particularly at the α- and β-positions with phenyl substituents, significantly increases the computed cross-section values, see Fig. 4. For example, BODIPY2 and BODIPY4 values, calculated using RI-CC2, show a significant increase in σ^{2PA}, reaching 11.00 GM and 17.71 GM, respectively. This enhancement is similarly observed in GADIPY derivatives, with GADIPY2 and GADIPY4 achieving computed σ^{2PA} values of 8.49 GM and 4.43 GM, respectively, although these are not as high as their BODIPY counterparts. For antimony-based derivatives, SBDIPY2 and SBDIPY4 display moderate improvements, with σ^{2PA} values of 2.79 GM and 2.09 GM, respectively, while BIDIPY2 and BIDIPY4 present values of 1.06 GM and 10.26 GM, illustrating a diverse range of effects based on substituent type and position.

The observed trends in the computed σ^{2PA} values using MN15 are similar to those using RI-CC2. However, it is observed that the MN15 values for the simple chromophores such as BODIPY, GADIPY, and halogen-substituted SBDIPY and BIDIPY derivatives are generally underestimated compared to their RI-CC2 counterparts (Fig. 4). This underestimation of TD-DFT results relative to RI-CC2 (and experiment) has been established in previous works.[78,91] In contrast, for the extended conjugated systems like BODIPY2, BODIPY4, GADIPY2, BIDIPY2, and BIDIPY4, the MN15 values are significantly higher than those obtained from RI-CC2. This has been observed in a study involving 48 organic molecules, where certain functionals yielded δ^{2PA} values higher than those determined by RI-CC2.[47] Here, where TD-DFT overestimates ΔE (even when compared to RI-CC2) for DIPYs, one might attribute the overestimation of σ^{2PA} to this effect, but the σ^{2PA} values computed by TD-DFT are not consistently higher for all DIPYs; only those with α/β substituents. This suggests that the MN15 method exhibits a larger sensitivity to extending the conjugation. For example, the base BODIPY chromophore has a σ^{2PA} of only 0.30 GM, but this value dramatically increases in its derivatives, BODIPY2 and BODIPY4, to 19.23 GM and 29.41 GM, respectively. Similarly, GADIPY2 shows a substantial increase to 14.54 GM, whereas GADIPY4 has a marginal enhancement to 1.74 GM. However, the SBDIPY derivatives do not follow this trend; SBDIPY2 and SBDIPY4 show relatively lower values of 1.48 GM and 0.13 GM, respectively, which is also observed using RI-CC2, thus, suggesting antimony's limited effectiveness as a boron replacement in this context. Meanwhile, BIDIPY derivatives present mixed results where BIDIPY2 has a modest σ^{2PA} of 1.41 GM, while the computed value of BIDIPY4 significantly increases to 16.37 GM. The variations in the computed values of σ^{2PA} observed with the MN15 functional are similarly reflected when using the other investigated functionals, see Table S3 (ESI†).

Since the transition strength, δ^{2PA}, is directly related to σ^{2PA} but excludes the dependency on ΔE, it enables a focused analysis for assessing the performance of functionals in predicting δ^{2PA}. The computed values of δ^{2PA} for the DIPY chromophores generally exhibit consistent trends across the investigated functionals. Similar to its performance in predicting σ^{2PA} trends, MN15 underestimates δ^{2PA} relative to RI-CC2 for the parent compounds such as BODIPY and GADIPY, as well as for the halogen-substituted derivatives. This underestimation is also observed for BIDIPY derivatives. However, for the extended conjugated systems, MN15 performs comparably or even overestimates δ^{2PA}. For example, the computed values for BODIPY2 and BODIPY4 using MN15 exceed those from RI-CC2. On the

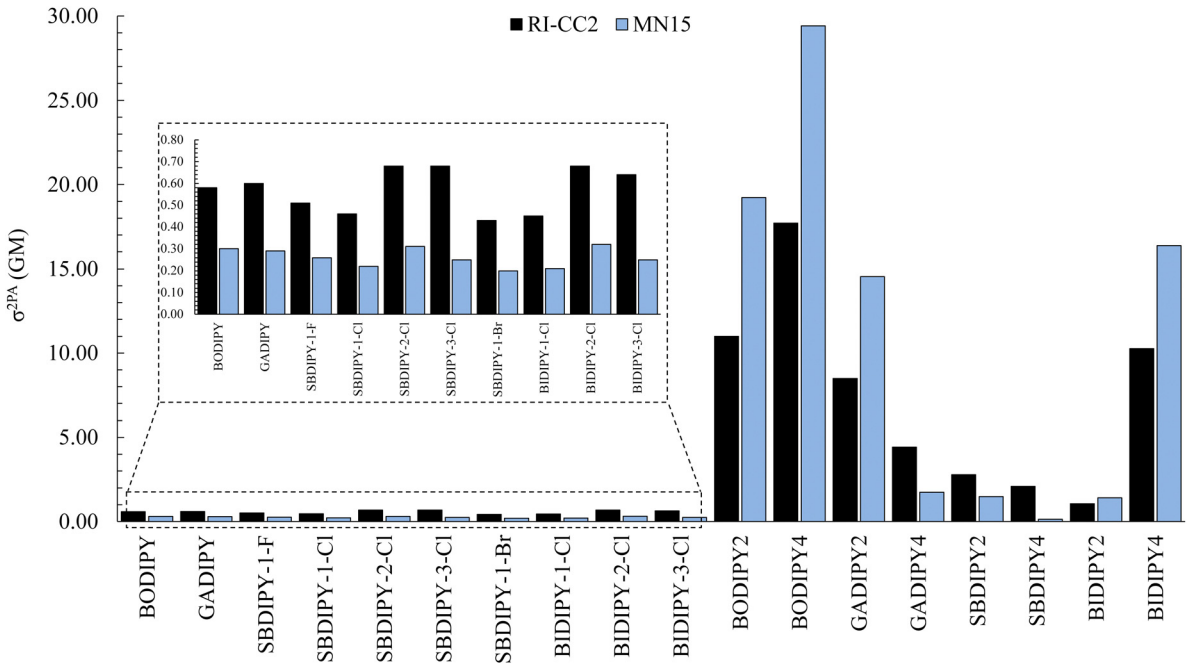

Fig. 4 The computed σ^{2PA} (GM) for the DIPY chromophores, at RI-CC2 and MN15. The computed absolute values are given in Table S3 (ESI†).

other hand, the MAE analysis of δ^{2PA} further shows the differences among the investigated functionals and their relative performance in predicting σ^{2PA}. Unlike its performance for σ^{2PA}, MN15 exhibits a larger MAE for δ^{2PA} compared to other functionals such as CAM-B3LYP and ωB97X. This reflects the sensitivity of MN15 to both the core atom and substituent effects, as previously observed for σ^{2PA}. Despite these deviations, the qualitative trends observed with MN15 generally agree with RI-CC2, particularly for systems with extended conjugation. This suggests that MN15 remains reliable for exploring the relative changes in both δ^{2PA} and σ^{2PA}. Overall, a key factor influencing the σ^{2PA} value and its computation is the calculated δ^{2PA}, which is highly dependent on the choice of functional.

The analysis of σ^{2PA} for the DIPY chromophores using RI-CC2 and MN15 reveals valuable insights into the effects of core atoms and substituents on their 2PA cross-sections. For example, the type of core atom influences σ^{2PA}, with BODIPY derivatives exhibiting the highest values, followed by GADIPY, BIDIPY, and SBDIPY. The type of core atom also impacts how σ^{2PA} increases upon substitution; although besides boron showing the largest increases and antimony the smallest, there are no clear trends. Moreover, the presence of phenyl groups at the chromophore core, particularly at the α- and β-positions, significantly increases σ^{2PA} values, with TD-DFT showing a higher sensitivity to these substituents compared to RI-CC2.

Dipole moments and σ^{2PA}

To elucidate the computed values of σ^{2PA} and their underlying behavior, we analyzed several dipole moments: the ground state (μ_{00}), excited state (μ_{11}), and transition (μ_{01}) dipole moments, as well as the change in permanent dipole moment ($\Delta\mu = \mu_{11} - \mu_{00}$). It is important to recognize that both μ_{00} and μ_{11} significantly influence $\Delta\mu$. Accurate calculation of μ_{00} alone is insufficient; an underestimated $\Delta\mu$ can still occur unless μ_{11} is also precisely computed. Thus, the accuracy of both values is essential for correctly determining $\Delta\mu$. These dipole moments critically affect the computed σ^{2PA} values *via* δ^{2PA} (eqn (2)) and δ_{0f}^{2PA} (eqn (6)). The influence of $\Delta\mu$ on σ^{2PA} has been substantiated both experimentally[38,99] and through computational methods using the two-state model,[48,91,100,101] which highlights the direct proportionality between σ^{2PA} and $\Delta\mu$. Furthermore, our recent study on a set of coumarins has shown that σ^{2PA} values correspond directly with μ_{01} across various solvents.[37] However, this relationship does not hold in the gas-phase,[46] indicating a contextual dependency of the validity of the two-state model for a given chromophore.

Overall, the calculated dipole moments, μ_{00}, μ_{11}, μ_{01}, and $\Delta\mu$, demonstrate various inconsistencies and do not correspond proportionally with the computed σ^{2PA} values (Tables S3–S5, ESI†), which has been previously observed.[46] However, it is observed that systems with larger cross-sections generally show higher dipole moment values, where for the basic DIPY chromophores, $\Delta\mu$ values remain below 0.50 D, whereas they exceed 1.00 D for the substituted ones. In particular, phenyl-substituted DIPYs, which have higher values of $\Delta\mu$, tend to have larger σ^{2PA} values. For example, the highest computed values of σ^{2PA} for BODIPY2 and BODIPY4, computed using RI-CC2, are 11.00 GM and 17.71 GM, respectively. These high values correspond to $\Delta\mu$ of 2.37 D and 3.88 D, the largest in the series, and these findings are consistent with those obtained using TD-DFT. Furthermore, similar observations are obtained in GADIPY2 and GADIPY4, where their σ^{2PA} (RI-CC2) values, are 8.49 GM and 4.43 GM, respectively, with $\Delta\mu$ values of 2.93 and 1.51 [D]. A similar trend is also observed in BIDIPY2 and BIDIPY4, see Tables S3 and S4 (ESI†).

Given that the dipole moments of these DIPY chromophores have not been previously studied, it becomes crucial to examine how different functionals perform in calculating their dipole moments. The performance of the examined functionals in predicting dipole moments was evaluated by comparing their computed MAEs relative to RI-CC2. Generally, the performance of these functionals does not qualitatively align with their prior performance in calculating values of ΔE and σ^{2PA}. Furthermore, the functionals' performance varies, with no single functional consistently performing best across all computed properties, see Fig. 5. In particular, the top-performing functionals, like MN15, typically do not show reliable performance in computing all the dipole moments.

The dipole moments assessment shows that the computed MAEs are generally low, with the maximum reaching only 1.00 [D], see Fig. 5. Consequently, considering the small magnitude of these MAEs, any of the selected functionals could feasibly be utilized for these property calculations. For example, M11 demonstrated a good performance for μ_{11}, μ_{00}, and $\Delta\mu$, with MAEs of 0.24, 0.30, and 0.36 [D], respectively (Tables S4 and S5, ESI†). However, it showed the least accuracy for μ_{01} (MAE = 1.04 [D]). In contrast, the MN15 functional most accurately predicted the values of μ_{00}, achieving a MAE of 0.13 [D]. However, its accuracy for excited state properties, μ_{11} and μ_{01}, was less reliable, which also affected its overall performance in calculating $\Delta\mu$.

On the other hand, the ωB97X functional showed consistent accuracy across the computed moments, with all MAEs remaining below 0.60 [D]. The MAEs for μ_{00} and μ_{11} were within 0.25 [D],

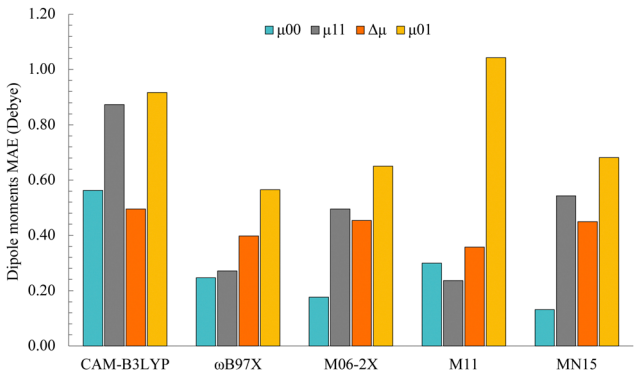

Fig. 5 The computed MAEs of μ_{00}, μ_{11}, μ_{01}, and $\Delta\mu$ ([D]) for the DIPY chromophores, relative to RI-CC2. The computed absolute values are given in Tables S4 and S5 (ESI†).

while μ_{01} and $\Delta\mu$ were found to be slightly higher with MAEs of 0.57 [D] and 0.40 [D], respectively. Similarly, M06-2X also displayed consistently good performance, with MAEs that were generally close in value to those observed for ωB97X. However, the one functional that showed the overall highest computed MAEs is CAM-B3LYP, with MAEs of μ_{11} and μ_{01} reaching up to 0.90 [D].

Conclusions

The 2PA properties of various substituted DIPY chromophores were analyzed using RI-CC2, CAM-B3LYP, ωB97X, M06-2X, M11, and MN15. A comprehensive examination of the computed values for σ^{2PA}, ΔE, μ_{00}, μ_{11}, μ_{01}, and $\Delta\mu$ was performed. The findings reveal that changing the core atom in the DIPY framework, from boron to heavier elements like gallium, antimony, and bismuth, results in negligible alterations to the σ^{2PA} values for the ''parent'' compounds. However, the introduction of phenyl substituents at the α- and β-positions significantly enhances the σ^{2PA} values. This behavior was consistently observed across all chromophores studied, at different levels of theory, where extended conjugation resulted in larger σ^{2PA} values. However, the identity of the core atom strongly influenced the relative increases seen in σ^{2PA} upon substitution. Thus, one cannot simply take substituted BODIPY frameworks with large σ^{2PA} and assume they will translate to large σ^{2PA} values for the GADIPY, SBDIPY, and BIDIPY analogues.

Unlike earlier research that largely focused on a single core atom type, we systematically examined a broad set of DIPY analogues substituted with heavier atoms and various phenyl groups. This approach reveals the complex interplay between the core atom and substituents; while phenyl substitutions greatly enhance σ^{2PA} in BODIPY, their impact is less uniform in heavy-core systems. By demonstrating that such modifications do not translate directly across different DIPY cores, our results establish that achieving optimal 2PA properties requires an integrated design regime that considers both the nature of the core atom and the positioning of substituents. This level of insight was not previously available and provides a more comprehensive framework for guiding the synthesis of new DIPY-based chromophores with enhanced 2PA performance.

Furthermore, the results demonstrated difficulties in precisely correlating σ^{2PA} with dipole moments; thus, highlighting the insufficiency of the two-state model in describing 2PA for these systems. The dipole moments (μ_{00}, μ_{11}, μ_{01}, and $\Delta\mu$) displayed several inconsistencies and often did not scale proportionally with the computed σ^{2PA} values. Despite these inconsistencies, systems with larger σ^{2PA} values showed significant changes in permanent dipole moments, particularly in phenyl-substituted DIPY chromophores and their $\Delta\mu$ values. Moreover, the results indicate that substitution at the α/β-positions improves σ^{2PA} values more significantly than substitution at the *meso*-position. These findings agree with earlier studies,[52,53,55,57] confirming the critical role of extended conjugation and symmetry in improving 2PA properties. Previous research has shown that modifications at the α- and β-positions effectively increase σ^{2PA} by promoting electron delocalization and extending the π-conjugated system.[52,53,55–57] Our current results reinforce these trends and further highlight that incorporating different core atoms, *e.g.*, Ga, Sb, Bi, combined with strategic α- and β-substitutions, can optimize 2PA properties.

Among the computational methods assessed, despite all functionals showing relatively low MAEs and slight relative differences, MN15 emerged as the superior functional in predicting both σ^{2PA} and ΔE values. Typically, TD-DFT predictions for σ^{2PA} are lower compared to those computed using RI-CC2; however, the values were notably higher for some of the investigated chromophores. This reveals the distinct electronic characteristics of the DIPY chromophores, which likely result in a unique interplay of excited-state properties influencing 2PA behavior. Moreover, this study is among the first to investigate both σ^{2PA} and δ^{2PA} values using the RI-CC2 method for these systems, establishing a reliable benchmark for TD-DFT results. This comprehensive computational analysis not only deepens our understanding of these novel chromophores but also emphasizes the critical role of wavefunction-based methods, such as RI-CC2, in accurately evaluating 2PA properties.

Author contributions

I. A. E.: conceptualization, data curation, formal analysis, investigation, validation, co-supervision, writing – original draft. M. Z.: data curation, investigation, visualization. A. B.: conceptualization, resources, funding acquisition, validation, supervision, writing – review & editing.

Data availability

The Cartesian coordinates of the optimized geometries, excitation energies, dipole moments, 2PA cross-sections, 2PA transition strengths, mean absolute errors, and mean signed errors are provided free of charge in the ESI.†

Conflicts of interest

There are no conflicts to declare.

Acknowledgements

I. A. E. acknowledges the support of the Natural Sciences and Engineering Research Council of Canada (NSERC) through a Postgraduate Scholarship–Doctoral (PGS D) award. M. Z. thanks the China Scholarship Council for the support of her internship at the University of Alberta. A. B. thanks NSERC for a Discovery Grant. This research was enabled in part by support provided by BC DRI Group and the Digital Research Alliance of Canada (alliancecan.ca).

References

1 R. Ziessel, G. Ulrich and A. Harriman, *New J. Chem.*, 2007, **31**, 496–501.
2 A. Loudet and K. Burgess, *Chem. Rev.*, 2007, **107**, 4891–4932.
3 A. Treibs and F.-H. Kreuzer, *Liebigs Ann. Chem.*, 1968, **718**, 208–223.
4 A. Schmitt, B. Hinkeldey, M. Wild and G. Jung, *J. Fluoresc.*, 2009, **19**, 755–758.
5 I. J. Arroyo, R. Hu, G. Merino, B. Z. Tang and E. Peña-Cabrera, *J. Org. Chem.*, 2009, **74**, 5719–5722.
6 G. Ulrich, R. Ziessel and A. Harriman, *Angew. Chem., Int. Ed.*, 2008, **47**, 1184–1201.
7 A. C. Benniston and G. Copley, *Phys. Chem. Chem. Phys.*, 2009, **11**, 4124–4131.
8 M. Kaur, A. Janaagal, N. Balsukuri and I. Gupta, *Coord. Chem. Rev.*, 2024, **498**, 215428.
9 S. K. Sarkar, S. Mukherjee and P. Thilagar, *Inorg. Chem.*, 2014, **53**, 2343–2345.
10 X.-D. Jiang, Y. Fu, T. Zhang and W. Zhao, *Tetrahedron Lett.*, 2012, **53**, 5703–5706.
11 R. Gresser, H. Hartmann, M. Wrackmeyer, K. Leo and M. Riede, *Tetrahedron*, 2011, **67**, 7148–7155.
12 Y. Hayashi, N. Obata, M. Tamaru, S. Yamaguchi, Y. Matsuo, A. Saeki, S. Seki, Y. Kureishi, S. Saito and S. Yamaguchi, *et al.*, *Org. Lett.*, 2012, **14**, 866–869.
13 A. Kamkaew, S. H. Lim, H. B. Lee, L. V. Kiew, L. Y. Chung and K. Burgess, *Chem. Soc. Rev.*, 2013, **42**, 77–88.
14 S. H. Alamudi, R. Satapathy, J. Kim, D. Su, H. Ren, R. Das, L. Hu, E. Alvarado-Martnez, J. Y. Lee and C. Hoppmann, *et al.*, *Nat. Commun.*, 2016, **7**, 11964.
15 A. B. Nepomnyashchii and A. J. Bard, *Acc. Chem. Res.*, 2012, **45**, 1844–1853.
16 G. Duran-Sampedro, A. R. Agarrabeitia, I. Garcia-Moreno, A. Costela, J. Bañuelos, T. Arbeloa, I. Lopez Arbeloa, J. L. Chiara and M. J. Ortiz, *Eur. J. Org. Chem.*, 2012, 6335–6350.
17 N. Boens, V. Leen and W. Dehaen, *Chem. Soc. Rev.*, 2012, **41**, 1130–1172.
18 M. S. T. Gonçalves, *Chem. Rev.*, 2009, **109**, 190–212.
19 L. Yuan, W. Lin, K. Zheng, L. He and W. Huang, *Chem. Soc. Rev.*, 2013, **42**, 622–661.
20 M. Vendrell, D. Zhai, J. C. Er and Y.-T. Chang, *Chem. Rev.*, 2012, **112**, 4391–4420.
21 W. Denk, J. H. Strickler and W. W. Webb, *Science*, 1990, **248**, 73–76.
22 J. Dipold, E. E. Romero, J. Donnelly, T. P. Calheiro, H. G. Bonacorso, B. A. Iglesias, J. P. Siqueira, F. E. Hernandez, L. De Boni and C. R. Mendonca, *Phys. Chem. Chem. Phys.*, 2019, **21**, 6662–6671.
23 P. Li, D. Sun, N. Liu, Y. Fang, C. P. Gros, F. Bolze and H.-J. Xu, *Dyes Pigm.*, 2021, **192**, 109418.
24 O. A. Chaves, T. P. Calheiro, J. C. Netto-Ferreira, M. C. de Oliveira, S. Z. Franceschini, C. M. C. de Salles, N. Zanatta, C. P. Frizzo, B. A. Iglesias and H. G. Bonacorso, *Int. J. Biol. Macromol.*, 2020, **160**, 1114–1129.
25 T. Bura, P. Retailleau, G. Ulrich and R. Ziessel, *J. Org. Chem.*, 2011, **76**, 1109–1117.
26 F. Heisig, S. Gollos, S. J. Freudenthal, A. El-Tayeb, J. Iqbal and C. E. Müller, *J. Fluoresc.*, 2014, **24**, 213–230.
27 I. F. Sengul, E. Okutan, H. Kandemir, E. Astarc and B. Çosut, *Dyes Pigm.*, 2015, **123**, 32–38.
28 Y. P. Rey, D. G. Abradelo, N. Santschi, C. A. Strassert and R. Gilmour, *Eur. J. Org. Chem.*, 2017, 2170–2178.
29 M. A. Filatov, *Org. Biomol. Chem.*, 2020, **18**, 10–27.
30 W. Wan, M. S. Silva, C. D. McMillen, S. E. Creager and R. C. Smith, *J. Am. Chem. Soc.*, 2019, **141**, 8703–8707.
31 A. Korzun, S. Crespi, C. Golz and A. Bismuto, *Chem. Sci.*, 2023, **14**, 6579–6584.
32 C. Liu, Y. Dai, Q. Han, C. Liu and Y. Su, *Chem. Commun.*, 2023, **59**, 2161–2164.
33 Q. Bao, Y. Dai, C. Liu, X. Liu, J. Xiao, D. Xu and Y. Su, *Eur. J. Inorg. Chem.*, 2024, e202300643.
34 Y. Dai, M. Bao, W. Wang, Z. Xie, C. Liu and Y. Su, *Chin. J. Chem.*, 2022, **40**, 2387–2392.
35 M. Göppert-Mayer, *Ann. Phys.*, 1931, **401**, 273–294.
36 S. Pascal, S. David, C. Andraud and O. Maury, *Chem. Soc. Rev.*, 2021, **50**, 6613–6658.
37 I. A. Elayan and A. Brown, *Phys. Chem. Chem. Phys.*, 2023, **25**, 16772–16780.
38 M. Drobizhev, N. S. Makarov, S. E. Tillo, T. E. Hughes and A. Rebane, *Nat. Methods*, 2011, **8**, 393–399.
39 M. Blanchard-Desce, *C. R. Phys.*, 2002, **3**, 439–448.
40 F. Helmchen and W. Denk, *Nat. Methods*, 2005, **2**, 932–940.
41 G. S. He, L.-S. Tan, Q. Zheng and P. N. Prasad, *Chem. Rev.*, 2008, **108**, 1245–1330.
42 M. Pawlicki, H. A. Collins, R. G. Denning and H. L. Anderson, *Angew. Chem., Int. Ed.*, 2009, **48**, 3244–3266.
43 D. Oulianov, I. Tomov, A. Dvornikov and P. Rentzepis, *Opt. Commun.*, 2001, **191**, 235–243.
44 M. De Wergifosse, A. L. Houk, A. I. Krylov and C. G. Elles, *J. Chem. Phys.*, 2017, **146**, 144305.
45 I. A. Elayan and A. Brown, *J. Phys. Chem. A*, 2024, **128**, 7511–7523.
46 I. A. Elayan, L. Rib, R. A. Mendes and A. Brown, *J. Chem. Theory Comput.*, 2024, **20**, 3879–3893.
47 M. Chołuj, M. M. Alam, M. T. Beerepoot, S. P. Sitkiewicz, E. Matito, K. Ruud and R. Zaleśny, *J. Chem. Theory Comput.*, 2022, **18**, 1046–1060.
48 M. T. Beerepoot, D. H. Friese, N. H. List, J. Kongsted and K. Ruud, *Phys. Chem. Chem. Phys.*, 2015, **17**, 19306–19314.
49 B. Tejendra, S. S. Rajput and M. M. Alam, *ChemPhysChem*, 2024, **25**, e202300710.
50 X. Liu, J. Zhang, K. Li, X. Sun, Z. Wu, A. Ren and J. Feng, *Phys. Chem. Chem. Phys.*, 2013, **15**, 4666–4676.
51 B. Küçüköz, G. Sevinç, E. Yildiz, A. Karatay, F. Zhong, H. Ylmaz, Y. Tutel, M. Hayval, J. Zhao and H. Yaglioglu, *Phys. Chem. Chem. Phys.*, 2016, **18**, 13546–13553.
52 L. W. Barros, T. A. Cardoso, A. Bihlmeier, D. Wagner, D. K. Kölmel, A. Hörner, S. Bräse, C. H. B. Cruz and L. A. Padilha, *Phys. Chem. Chem. Phys.*, 2017, **19**, 21683–21690.

53 J. Yang, Y. Rousselin, L. Bucher, N. Desbois, F. Bolze, H.-J. Xu and C. P. Gros, *ChemPlusChem*, 2018, **83**, 838–844.
54 P. Didier, G. Ulrich, Y. Mély and R. Ziessel, *Org. Biomol. Chem.*, 2009, **7**, 3639–3642.
55 B. Sui, M. V. Bondar, D. Anderson, H. J. Rivera-Jacquez, A. E. Masunov and K. D. Belfield, *J. Phys. Chem. C*, 2016, **120**, 14317–14329.
56 S. Pascal, Q. Bellier, S. David, P.-A. Bouit, S.-H. Chi, N. S. Makarov, B. Le Guennic, S. Chibani, G. Berginc, P. Feneyrou, D. Jacquemin, J. W. Perry, O. Maury and C. Andraud, *J. Phys. Chem. C*, 2019, **123**, 23661–23673.
57 G. Song, Z. Li, Y. Han, J. Jia, W. Zhou, X. Zhang, Y. Wang and Y. Song, *Molecules*, 2022, **27**, 2849.
58 O. Christiansen, H. Koch and P. Jørgensen, *Chem. Phys. Lett.*, 1995, **243**, 409–418.
59 D. H. Friese, C. Hättig and K. Ruud, *Phys. Chem. Chem. Phys.*, 2012, **14**, 1175–1184.
60 A. D. Becke, *J. Chem. Phys.*, 1993, **98**, 5648–5652.
61 C. Lee, W. Yang and R. G. Parr, *Phys. Rev. B: Condens. Matter Mater. Phys.*, 1988, **37**, 785.
62 T. Yanai, D. P. Tew and N. C. Handy, *Chem. Phys. Lett.*, 2004, **393**, 51–57.
63 J.-D. Chai and M. Head-Gordon, *J. Chem. Phys.*, 2008, **128**, 084106.
64 Y. Zhao and D. G. Truhlar, *Theor. Chem. Acc.*, 2008, **120**, 215–241.
65 R. Peverati and D. G. Truhlar, *J. Phys. Chem. Lett.*, 2011, **2**, 2810–2817.
66 S. Y. Haoyu, X. He, S. L. Li and D. G. Truhlar, *Chem. Sci.*, 2016, **7**, 5032–5051.
67 S. Grimme, A. Hansen, S. Ehlert and J.-M. Mewes, *J. Chem. Phys.*, 2021, **154**, 064103.
68 C. Adamo and V. Barone, *J. Chem. Phys.*, 1999, **110**, 6158–6170.
69 M. J. Frisch, G. W. Trucks, H. B. Schlegel, G. E. Scuseria, M. A. Robb, J. R. Cheeseman, G. Scalmani, V. Barone, G. A. Petersson, H. Nakatsuji, X. Li, M. Caricato, A. V. Marenich, J. Bloino, B. G. Janesko, R. Gomperts, B. Mennucci, H. P. Hratchian, J. V. Ortiz, A. F. Izmaylov, J. L. Sonnenberg, D. Williams-Young, F. Ding, F. Lipparini, F. Egidi, J. Goings, B. Peng, A. Petrone, T. Henderson, D. Ranasinghe, V. G. Zakrzewski, J. Gao, N. Rega, G. Zheng, W. Liang, M. Hada, M. Ehara, K. Toyota, R. Fukuda, J. Hasegawa, M. Ishida, T. Nakajima, Y. Honda, O. Kitao, H. Nakai, T. Vreven, K. Throssell, J. A. Montgomery, Jr., J. E. Peralta, F. Ogliaro, M. J. Bearpark, J. J. Heyd, E. N. Brothers, K. N. Kudin, V. N. Staroverov, T. A. Keith, R. Kobayashi, J. Normand, K. Raghavachari, A. P. Rendell, J. C. Burant, S. S. Iyengar, J. Tomasi, M. Cossi, J. M. Millam, M. Klene, C. Adamo, R. Cammi, J. W. Ochterski, R. L. Martin, K. Morokuma, O. Farkas, J. B. Foresman and D. J. Fox, *Gaussian 16, Revision C.01*, Gaussian, Inc., Wallingford CT, 2016.
70 M. R. Momeni and A. Brown, *J. Chem. Theory Comput.*, 2015, **11**, 2619–2632.
71 E. Runge and E. K. Gross, *Phys. Rev. Lett.*, 1984, **52**, 997.
72 M. E. Casida, *Recent Advances In Density Functional Methods: (Part I)*, World Scientific, 1995, pp. 155–192.
73 R. Ahlrichs, M. Bär, M. Häser, H. Horn and C. Kölmel, *Chem. Phys. Lett.*, 1989, **162**, 165–169.
74 S. G. Balasubramani, G. P. Chen, S. Coriani, M. Diedenhofen, M. S. Frank, Y. J. Franzke, F. Furche, R. Grotjahn, M. E. Harding and C. Hättig, *et al.*, *J. Chem. Phys.*, 2020, **152**, 184107.
75 F. Furche, R. Ahlrichs, C. Hättig, W. Klopper, M. Sierka and F. Weigend, *Wiley Interdiscip. Rev.: Comput. Mol. Sci.*, 2014, **4**, 91–100.
76 T. H. Dunning Jr, *J. Chem. Phys.*, 1989, **90**, 1007–1023.
77 D. E. Woon and T. H. Dunning Jr, *J. Chem. Phys.*, 1995, **103**, 4572–4585.
78 D. Grabarek and T. Andruniów, *J. Chem. Theory Comput.*, 2018, **15**, 490–508.
79 A. Klamt and G. Schüürmann, *J. Chem. Soc., Perkin Trans. 2*, 1993, 799–805.
80 S. Chibani, B. Le Guennic, A. Charaf-Eddin, O. Maury, C. Andraud and D. Jacquemin, *J. Chem. Theory Comput.*, 2012, **8**, 3303–3313.
81 S. Chibani, B. Le Guennic, A. Charaf-Eddin, A. D. Laurent and D. Jacquemin, *Chem. Sci.*, 2013, **4**, 1950–1963.
82 B. Le Guennic, O. Maury and D. Jacquemin, *Phys. Chem. Chem. Phys.*, 2012, **14**, 157–164.
83 F. Santoro and D. Jacquemin, *Wiley Interdiscip. Rev.: Comput. Mol. Sci.*, 2016, **6**, 460–486.
84 P.-F. Loos and D. Jacquemin, *ChemPhotoChem*, 2019, **3**, 684–696.
85 M. Feldt and A. Brown, *J. Comput. Chem.*, 2021, **42**, 144–155.
86 R. R. Birge and B. M. Pierce, *J. Chem. Phys.*, 1979, **70**, 165–178.
87 C. Hättig, O. Christiansen and P. Jørgensen, *J. Chem. Phys.*, 1998, **108**, 8331–8354.
88 S. Sirimatayanant and T. Andruniów, *J. Chem. Phys.*, 2023, **158**, 094106.
89 C. Naim, R. Zaleśny and D. Jacquemin, *J. Chem. Theory Comput.*, 2024, **20**, 9093–9106.
90 M. A. Salem and A. Brown, *J. Chem. Theory Comput.*, 2014, **10**, 3260–3269.
91 M. Rossano-Tapia and A. Brown, *Wiley Interdiscip. Rev.: Comput. Mol. Sci.*, 2022, **12**, e1557.
92 K. Ahmadzadeh, X. Li, Z. Rinkevicius, P. Norman and R. Zaleśny, *J. Phys. Chem. Lett.*, 2024, **15**, 969–974.
93 T. Schwabe, M. T. Beerepoot, J. M. H. Olsen and J. Kongsted, *Phys. Chem. Chem. Phys.*, 2015, **17**, 2582–2588.
94 K. D. Nanda and A. I. Krylov, *J. Chem. Phys.*, 2015, **142**, 064118.
95 Q. Alkhatib, W. Helal and A. Marashdeh, *RSC Adv.*, 2022, **12**, 1704–1717.
96 W. Helal, Q. Alkhatib and M. Gharaibeh, *Comput. Theor. Chem.*, 2022, **1207**, 113531.
97 W. Helal, A. Marashdeh, Q. Alkhatib, H. Qashmar, M. Gharaibeh and A. T. Afaneh, *Int. J. Quantum Chem.*, 2022, **122**, e27000.

98 C. Adamo and D. Jacquemin, *Chem. Soc. Rev.*, 2013, **42**, 845–856.
99 M. Drobizhev, N. S. Makarov, A. Rebane, G. de la Torre and T. Torres, *J. Phys. Chem. C*, 2008, **112**, 848–859.
100 M. A. Salem, I. Twelves and A. Brown, *Phys. Chem. Chem. Phys.*, 2016, **18**, 24408–24416.
101 D. Grabarek and T. Andruniów, *Int. J. Quantum Chem.*, 2020, **120**, e26086.